第 48 卷 第 21 期/2021 年 11 月/中国激光 研究论文

中国激光

光声显微成像引导注射微整形术研究

张芬[1,2]，张吴昱[1,2]，李春澍[1,2]，童壮壮[1,2]，马远征[1,2]，熊科迪[1,2*]

[1]华南师范大学生物光子学研究院，激光生命科学教育部重点实验室暨激光生命科学研究所，广东 广州 510631；

[2]华南师范大学生物光子学研究院，广东省激光生命科学重点实验室，广东 广州 510631

摘要 注射微整形手术中可能会出现经皮针头扎破面部动脉血管的情况，这会导致注射药物（如玻尿酸）渗入血管形成栓子、引发血管栓塞，从而致使局部组织缺血、失明甚至中风。为解决这一问题，提出利用光声显微成像引导注射微整形手术。利用带有导针器的光声显微成像探头对固定角度插入的注射针头成像，得到针头的行进路线，然后对目标区域进行三维血管成像，通过图像融合并提取其中针头与血管相交区域的像素点数量，可判断针头是否会扎破面部动脉血管，降低手术风险。通过叶脉和活体小鼠成像实验验证了该方法的可行性，结果表明，该方法可以精确地引导扎针，在提高注射微整形手术安全性方面有良好的应用前景。

关键词 生物光学；光声显微成像；手术导航；注射微整形术；图像融合

中图分类号 Q631 **文献标志码** A **doi**：10.3788/CJL202148.2107002

1 引 言

注射微整形是最常见的微整形手术之一，通过在人体特定部位注射与人体相容性较高的材料来实现美容效果[1-2]，其中最常用的是玻尿酸。玻尿酸是人体真皮组织中的重要成分，有不溶于水、不易在组织中发生转移、代谢率低及高保水等特点，其随着人年龄的增长而流失，皮肤因此产生皱纹。将玻尿酸注射在皱纹凹陷下部的真皮的中、深层，可以补偿人体缺失的玻尿酸，达到除皱的效果[3]。据不完全统计，玻尿酸注射后严重并发症的发生率约为0.06%[4-5]，包括局部组织缺血、失明、中风等[6-7]，其中大部分是由于手术时针头意外扎破面部动脉血管（直径约为 100 ～ 1900 μm）[8-10]，玻尿酸进入血液循环系统所致。因此，利用医学影像技术实现人体面部血管的可视化，能够提高注射微整形手术的安全性。

传统的医学影像技术中，超声成像利用生物组织的声阻抗差异进行成像，图像对比度较差，分辨率不高，难以清晰地成像出皮肤真皮层的血管网络[11]；光学显微成像能够得到分辨率较高的图像，但受限于生物组织对光的强散射作用，成像深度往往小于 1 mm，难以检测到皮肤真皮层的血管[12]。光声成像（PAI）是一种基于光学吸收差异、以超声波为信息载体的高特异性、高对比度的介观成像方法[13]，它结合了光学成像的高分辨率与超声成像的深穿透深度，在生物医学成像领域得到了广泛的研究[14-16]。作为光声成像领域的重要分支，光声显微成像（PAM）通过光（声）焦点在成像区域内逐点扫描的方式，利用血红蛋白天然地对绿光（532 nm）具有高吸收特性，可无损无标记地获取人体皮肤真皮层血管的高分辨率、高对比度图像[17-19]。

本文用叶脉模拟皮肤真皮层的血管网络结构，分别对注射针头、叶脉进行光声显微成像，通过二者的三维融合图像判断针头行进路线与叶脉主干（直径大于 100 μm）的相对位置，引导针头避开叶脉主干。并且进行了扎针实验，所得结果与融合图像预测的结果一致，证明了光声显微成像引导注射微整形手术的可行性。另外，本文对活体大鼠耳朵上的血管进行三维成像，并将成像结果与注射针头的三

收稿日期：2021-00-00；**修回日期**：2021-00-00；**录用日期**：2021-00-00

基金项目：国家自然科学基金（62005084，61822505，11774101，61627827）、广东省自然科学基金（2019A1515011399）、中国博士后科学基金（2019M652943）

通信作者：*xiongkd2012@163.com

维图像进行融合。通过统计融合图像中针头与血管相交区域的像素点数量，定量地引导针头避开直径大于 100 μm 的血管。

2　基本原理与实验装置

利用光声显微成像引导注射微整形手术的原理如图 1 所示，针头被约束在导针器上的导针孔中，首先采集约束在导针器上的针头（康德莱微整形针头 25G，直径 500 μm）的光声数据，得到固定角度针头的三维光声图像，即针头的行进路线。然后取出针头，采集目标皮肤区域血管的光声数据，得到真皮层血管网络的三维光声图像。需要注意的是，玻尿酸注射引发的并发症中，大部分是由针头意外扎破面部动脉血管（直径约为 100～1900 μm）引起的，所以本文重点关注直径 100 μm 以上的血管。融合血管网络与针头的三维图像，若针头与直径 100 μm 以上的血管相交，表明针头进入目标区域皮肤后，扎破此血管并引起并发症的可能性高，此时应移动探头，重新寻找注射位置。若融合图像中针头与直径 100 μm 以上的血管错开，表明针头会避开此血管，能够在此位置入针注射玻尿酸，引导结束。

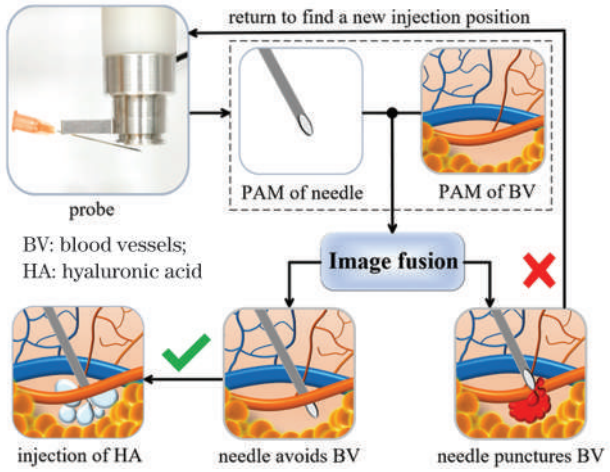

图 1　光声显微成像引导注射微整形手术原理图

Fig. 1　Schematic of photoacoustic microscopy for injection navigation of micro-plastic surgery

本文中使用的光声显微系统[20-21]如图 2 所示，532 nm 激光器（Mosquitoo X 532-2-V，InnoLas）产生的脉冲激光（脉宽 12 ns）经过光学滤波及准直后入射给微机电系统（MEMS）扫描镜（13Z2.1-3000，Mirrorcle Technologies Inc），然后被 4 倍平场物镜（RMS4，Thorlabs）聚焦到目标区域，激发光声信号。样品产生的光声信号被 45°放置的玻璃薄片（厚度：100 μm）反射至晶片直径为 6 mm、中心频率为 15 MHz 的平面超声换能器。超声换能器收集到的光声信号经过放大器（50 dB 增益，LNA-650，RFBAY）的放大后被高速数字采集卡（M4i.4450-x8，Spectrum）采集并存储至计算机中。MEMS 扫描镜由 FPGA 驱动，进行二维扫描，最终的成像范围为直径 5 mm 的圆形区域。实验过程中，水作为超声耦合介质，被透明薄膜封在探头中，系统的最佳横向分辨率为 8.9 μm，最佳轴向分辨率为 113 μm，成像一幅直径为 5 mm 的圆形区域图像所需的时间为 16 s[20-21]。正常成人的面部皮肤厚度值（表皮＋真皮）区间约为 1 ～ 3 mm[22-23]。针头、导针器和真皮层血管网络三者的位置关系如图 2 中虚线方框所示，导针器内导针孔的直径为 500 μm，根据导针孔的结构设计，完全入针后，针尖距离样品表面的垂直深度约为 1.5 mm，此深度在面部皮肤真皮中、深层的深度范围之内。

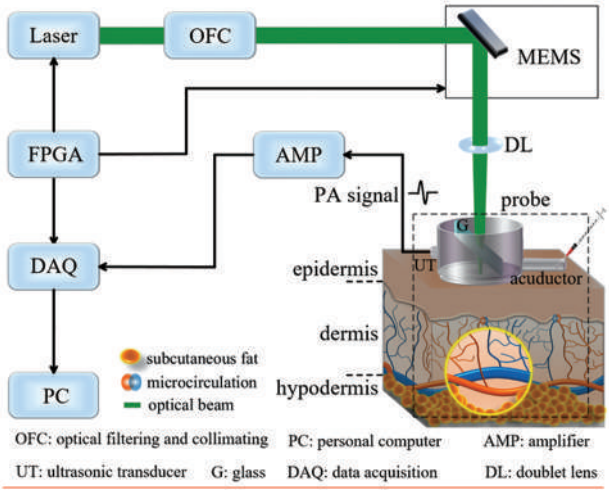

图 2　光声显微导航系统

Fig. 2　Photoacoustic microscopy navigation system.

使用基于 LabVIEW（2019，National Instruments，USA）自主编写的程序对原始数据进行低通滤波、小波变换处理后，重建血管图像。使用软件 ImageJ（National Institutes of Health，USA）得到三维图像并进行图像融合。使用基于 MATLAB（R2019b，the MathWorks，USA）的自主编写算法统计融合图像中针头与血管相交区域的像素点数量，其算法流程图如图 3 所示。输入针头和样品的数据矩阵 ***A*** 和 ***B***，对 ***A*** 和 ***B*** 进行二值化处理和三维盒式滤波，基于参考线融合矩阵 ***A*** 和 ***B*** 并做乘法运算，最后得到相交矩阵 ***C***，输出 ***C*** 的像素点数量。

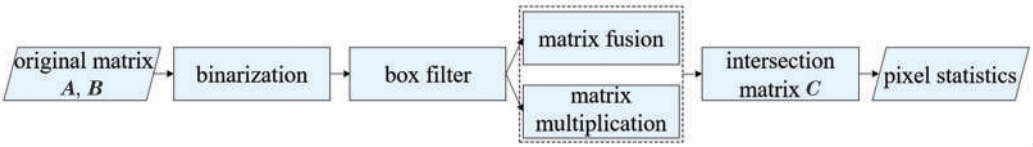

图 3 图像融合统计相交区域像素点数量的算法流程图

Fig. 3 Algorithm flow chart of image fusion to count numbers of pixels in intersection area

3 实验结果

为了验证光声显微成像引导注射微整形手术的可行性，设计了针头与叶脉的光声显微成像引导实验。叶脉被用来模拟皮肤真皮层的血管网络，其中，叶脉主干的直径约为 300～500 μm（模拟面部动脉），叶脉分支的直径在 100 μm 以下（模拟毛细血管网络）。分别对针头和叶脉进行成像，实验结果如图 4(a)所示，从左到右依次是针头、叶脉 1、叶脉 2 的三维光声图像。观察针头的图像，发现只得到了针头的上表面信息，为了判断针头与叶脉主干的相对位置，根据针尖的位置用虚线补全针头。图 4(b)显示了针头扎到叶脉主干的图像融合结果与扎针实验结果，此叶脉对应图 4(a)中的叶脉 1，融合图像中，针头穿过了叶脉主干。扎针实验结果中，针头扎到了叶脉主干，与融合图像预测的结果一致。图 4(c)显示了针头避开叶脉主干的图像融合结果与扎针实验结果，此叶脉对应图 4(a)中的叶脉 2，融合图像中，针头避开了叶脉主干。扎针实验结果中，针头避开了叶脉主干，与融合图像预测的结果一致。该实验结果显示，光声显微成像能够预测针头与模拟面部动脉（叶脉）的相对位置，以引导注射微整形手术。注意到，图 4(c)显示的融合图像与扎针图像中，针头扎进叶脉的位置有部分差异，其可能的原因是扎针实验中，针头挤压了固定叶脉的琼脂，使得叶脉发生轻微形变。

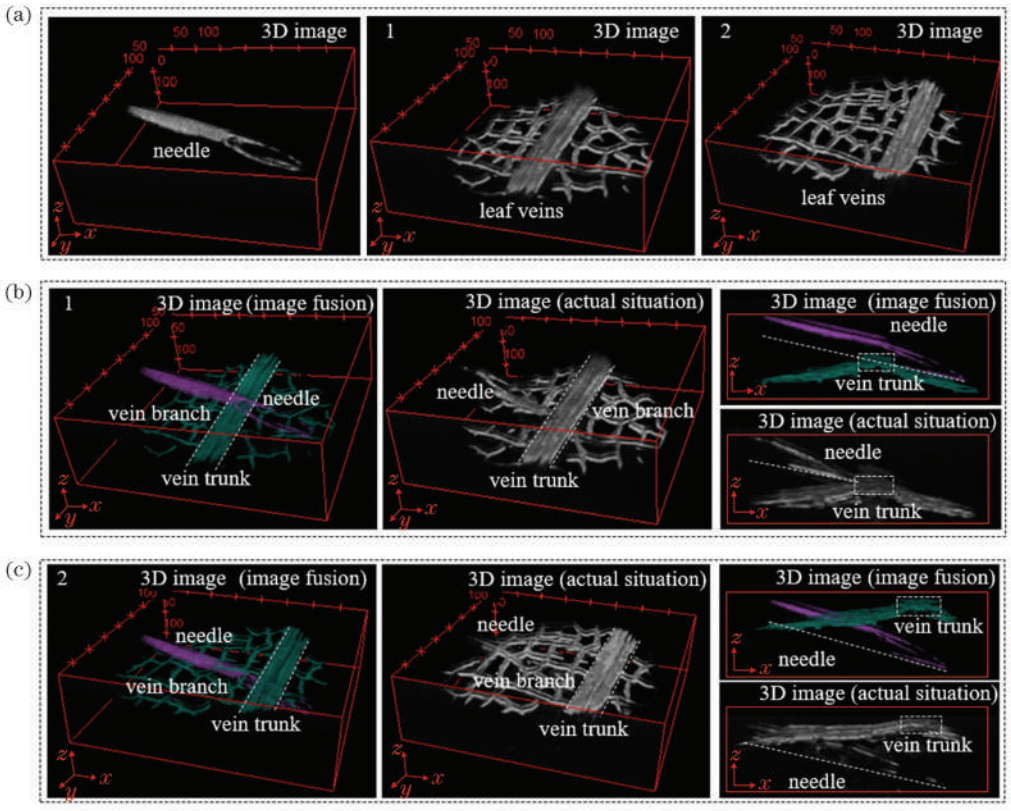

图 4 针头与叶脉的光声显微成像引导实验结果。(a)针头与不同叶脉的三维光声图像；(b)针头扎到叶脉主干的三维图像融合与实际情况；(c)针头避开叶脉主干的三维图像融合与实际情况

Fig. 4 Photoacoustic microscopy navigation results of needle and leaf veins. (a) Three-dimensional (3D) photoacoustic images of needle and leaf veins; (b) 3D image fusion and actual situation of needle puncturing vein trunk; (c) 3D image fusion and actual situation of needle avoiding vein trunk

进一步地，为了证明光声显微成像定量地引导注射微整形手术的能力，设计了针头与大鼠耳朵血管的光声显微成像引导实验。图 5(a)是针头的三维光声图像，图 5(b)是大鼠耳朵血管的三维光声图像。针头和血管的三维融合图像如图 5(c)所示，针头与主干血管(直径大于 100 μm)相交。通过透明化处理针头和血管图像并保持两者相交区域的颜色深度不变，可以凸显图像融合的相交区域，图 5(d)是经过透明化处理后的图像融合结果，图中的内插图显示了血管与针头相交区域的放大图。

移动样品矩阵以模拟样品的移动，图 5(e)是血管的最大值投影图像，血管与针头相交的初始位置[对应图 5(c)]位于图 5(e)的位置 1，图中 MAP 为最大投影。根据人体面部动脉的直径特点，人为选取 5 个位置，被选位置 4 处的血管为主干血管，被选位置 2 和被选位置 5 处的血管为毛细血管，被选位置 3 和被选位置 6 相对特殊，没有血管。分别融合针头和这些位置的血管，统计出相交区域的像素点数量如图 5(f)所示，主干血管(位置 1、4)与针头相交的像素点数量最多，分别为 35 和 31，毛细血管(位置 2、5)次之，分别为 8 和 5，没有血管的位置(位置 3、6)与针头相交的像素点数量为 0。该统计结果显示，根据相交区域像素点数量的大小，可以定量地判断针头是否会扎到主干血管。

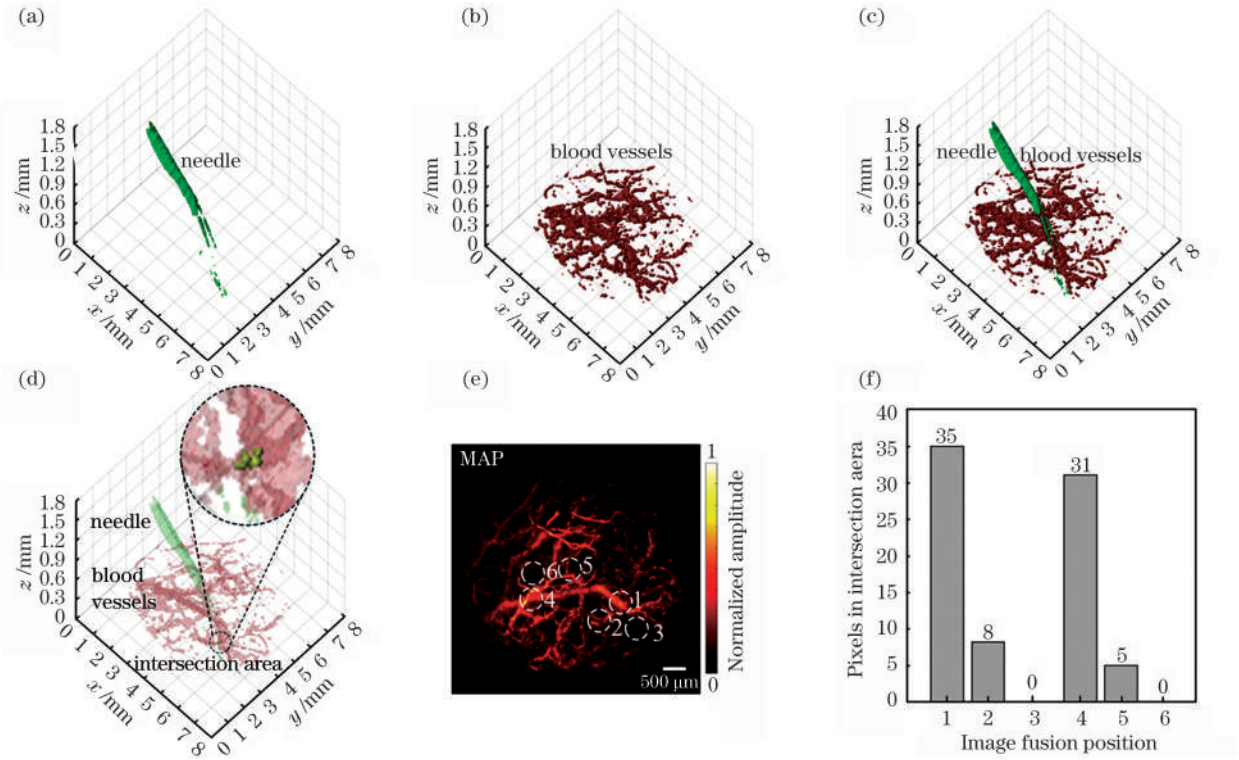

图 5 针头与活体大鼠耳朵血管的光声显微成像引导实验结果。(a)针头的三维光声图像；(b)血管的三维光声图像；(c)未透明化处理针头扎到血管的图像融合；(d)透明化处理后针头扎到血管的图像融合(插图：针头与血管相交区域的放大图)；(e)血管的最大值投影；(f)血管与针头相交区域的像素点数量统计图

Fig. 5 Photoacoustic microscopy navigation results of needle and rat ear blood vessels *in vivo*. (a) 3D photoacoustic image of needle; (b) 3D image of blood vessels; (c) image fusion of needle puncturing blood vessels without transparent processing; (d) image fusion of needle puncturing blood vessels with transparent processing (inset is enlarged view of intersection area between needle and blood vessels); (e) maximum projection of blood vessels; (f) pixel statistical map of intersection area of needle and blood vessels

4 结 论

叶脉实验结果表明，光声显微成像能够预测针头与模拟血管的相对位置，引导针头在安全区域入针。活体小鼠耳朵实验结果表明，根据相交区域的像素点数量，还能够定量地判断若按照导航路线扎入样品，针头将会扎到的血管类型，从而决策是否安全入针注射。综上所述，这项工作有望实现注射微整形手术的术前导航，对提高注射微整形手术安全性有良好的应用前景，然而还有一些需要改进的地方。本文所用的激光波长为 532 nm，这是由于血液天然地对此波长的激光具有高吸收特性[24-25]，但是，

由于生物组织对光的强散射，系统的成像深度受到了限制[24]，被成像大鼠耳朵厚度小于 1.5 mm，需要借助水槽、透明膜和水弥补厚度差，无法在大鼠耳朵上进行真实扎针实验。接下来，计划采用更长波长的激光（如 1064 nm），实现更大的穿透深度[26]。受所用系统光激发模式的限制，目前只能提取出针头的上表面信息，判断针头是否接触到了血管需要借助后处理算法。下一步，可以根据针头的真实尺寸仿真完整针头以提高实验精度。另外，注射位置的选取存在一定的盲目性，需要反复移动探头，大的成像视野与快的成像速度有助于提高检测效率。受成像速度的限制，所用的系统目前只能实现术前导航，而非术中导航，无法对针头进入样品的过程进行实时监控。后续的工作将会围绕以上几个问题进行改进。

参 考 文 献

[1] Devgan L, Singh P, Durairaj K. Minimally invasive facial cosmetic procedures [J]. Otolaryngologic Clinics of North America, 2019, 52(3): 443-459.

[2] Chuang J, Barnes C, Wong B J F. Overview of facial plastic surgery and current developments[J]. Surgery Journal (New York, N.Y.), 2016, 2(1): e17-e28.

[3] Matarasso S L, Carruthers J D, Jewell M L, et al. Consensus recommendations for soft-tissue augmentation with nonanimal stabilized hyaluronic acid (Restylane) [J]. Plastic and Reconstructive Surgery, 2006, 117(3): 3S-34S.

[4] Joganathan V, Shah-Desai S. Awareness of management of hyaluronic acid induced visual loss: a British national survey [J]. Eye, 2020, 34(12): 2280-2283.

[5] Bray D, Hopkins C, Roberts D N. A review of dermal fillers in facial plastic surgery [J]. Current Opinion in Otolaryngology & Head and Neck Surgery, 2010, 18(4): 295-302.

[6] Tansatit T, Apinuntrum P, Phetudom T. Periorbital and intraorbital studies of the terminal branches of the ophthalmic artery for periorbital and glabellar filler placements [J]. Aesthetic Plastic Surgery, 2017, 41(3): 678-688.

[7] Loh K T D, Phoon Y S, Phua V, et al. Successfully managing impending skin necrosis following hyaluronic acid filler injection, using high-dose pulsed hyaluronidase [J]. Plastic and Reconstructive Surgery. Global Open, 2018, 6(2): e1639.

[8] Carruthers J D A, Fagien S, Rohrich R J, et al. Blindness caused by cosmetic filler injection: a review of cause and therapy[J]. Plastic and Reconstructive Surgery, 2014, 134(6): 1197-1201.

[9] Lee S H, Gil Y C, Choi Y J, et al. Topographic anatomy of the superior labial artery for dermal filler injection [J]. Plastic and Reconstructive Surgery, 2015, 135(2): 445-450.

[10] Lee S H, Ha T J, Koh K S, et al. External and internal diameters of the facial artery relevant to intravascular filler injection [J]. Plastic and Reconstructive Surgery, 2019, 143(4): 1031-1037.

[11] Chang J H, Kim H H, Lee J, et al. Frequency compounded imaging with a high-frequency dual element transducer[J]. Ultrasonics, 2010, 50(4/5): 453-457.

[12] Xi P, Liu Y J, Yao Z R, et al. Optical imaging techniques in skin imaging diagnosis [J]. Chinese Journal of Lasers, 2011, 38(2): 0201001.
席鹏, 刘宇嘉, 姚志荣, 等. 用于皮肤影像诊断的光学成像方法[J]. 中国激光, 2011, 38(2): 0201001.

[13] Xu M H, Wang L V. Photoacoustic imaging in biomedicine [J]. Review of Scientific Instruments, 2006, 77(4): 041101.

[14] Wu H Q, Wang H Y, Xie W M, et al. Potential applications of photoacoustic imaging in early cancer diagnosis and treatment[J]. Laser & Optoelectronics Progress, 2019, 56(7): 070001.
吴华钦, 王昊宇, 谢文明, 等. 光声成像技术在早期癌症检测治疗中的潜在应用[J]. 激光与光电子学进展, 2019, 56(7): 070001.

[15] Wang L V, Hu S. Photoacoustic tomography: *in vivo* imaging from organelles to organs[J]. Science, 2012, 335(6075): 1458-1462.

[16] Liu Q, Jin T, Chen Q, et al. Research progress of miniaturized photoacoustic imaging technology in biomedical field[J]. Chinese Journal of Lasers, 2020, 47(2): 0207019.
刘强, 金天, 陈倩, 等. 小型化光声成像技术在生物医学领域的研究进展[J]. 中国激光, 2020, 47(2): 0207019.

[17] Wang Z Y, Yang F, Ma H G, et al. Photoacoustic and ultrasound (PAUS) dermoscope with high sensitivity and penetration depth by using a bimorph transducer[J]. Journal of Biophotonics, 2020, 13(9): e202000145.

[18] Chen C J, Yang S H, Xing D. Progress and application of photoacoustic microscopy technique [J]. Chinese Journal of Lasers, 2018, 45(3): 0307008.
陈重江, 杨思华, 邢达. 光声显微成像技术研究进展及其应用[J]. 中国激光, 2018, 45(3): 0307008.

[19] Long X Y, Tian C. Biomedical photoacoustic

microscopy: advances in technology and applications[J]. Chinese Journal of Lasers, 2020, 47(2): 0207016.
龙晓云, 田超. 生物医学光声显微成像: 技术和应用进展[J]. 中国激光, 2020, 47(2): 0207016.

[20] Zhang W Y, Ma H G, Cheng Z W, et al. Miniaturized photoacoustic probe for *in vivo* imaging of subcutaneous microvessels within human skin[J]. Quantitative Imaging in Medicine and Surgery, 2019, 9(5): 807-807.

[21] Zhang W Y, Ma H G, Cheng Z W, et al. High-speed dual-view photoacoustic imaging pen [J]. Optics Letters, 2020, 45(7): 1599-1602.

[22] Feng Y Q, Wang D C, Wang Y B, et al. Facial skin thickness distribution of Chinese young adults [J]. Chinese Journal of Aesthetic Medicine, 2007, 16(11): 1565-1568.
冯永强, 王德昌, 王一兵, 等. 青壮年面部皮肤厚度的分布特点[J]. 中国美容医学, 2007, 16(11): 1565-1568.

[23] Li Y N, Li Z X, Lu Y H, et al. Measure of skin thickness and study of skin sonogram in adult by high-frequency ultrasound [J]. Chinese Journal of Medical Imaging Technology, 2008, 24(10): 1622-1624.
李艳宁, 李智贤, 卢月华, 等. 高频超声对正常成人皮肤厚度测量及声像研究[J]. 中国医学影像技术, 2008, 24(10): 1622-1624.

[24] Hale G M, Querry M R. Optical constants of water in the 200-nm to 200-microm wavelength region[J]. Applied Optics, 1973, 12(3): 555-563.

[25] Cai Z L, Chen Z C, Wang W Z. Near-infrared absorption property of biological soft tissue constituents[J]. Journal of Medical & Biological Engineering, 2001, 21(1): 7-14.

[26] Homan K, Kim S, Chen Y S, et al. Prospects of molecular photoacoustic imaging at 1064 nm wavelength[J]. Optics Letters, 2010, 35(15): 2663-2665.

Photoacoustic Microscopy for Injection Navigation of Microplastic Surgery

Zhang Fen[1,2], Zhang Wuyu[1,2], Li Chunshu[1,2], Tong Zhuangzhuang[1,2], Ma Yuanzheng[1,2], Xiong Kedi[1,2*]

[1] *MOE Key Laboratory of Laser Life Science & Institute of Laser Life Science, College of Biophotonics, South China Normal University, Guangzhou, Guangdong* 510631, *China*;

[2] *Guangdong Provincial Key Laboratory of Laser Life Science, College of Biophotonics, South China Normal University, Guangzhou, Guangdong* 510631, *China*

Abstract

Objective In microplastic surgery, hyaluronic acid is injected into the dermis layer under the wrinkle depression to achieve the wrinkle removal effect. However, the percutaneous needle can puncture facial arteries, causing the penetration of hyaluronic acid into the blood vessels to form emboli and induce vascular embolism, resulting in local tissue ischaemia, blindness, and even stroke. The visualisation of human facial blood vessels can solve this problem. Photoacoustic imaging is a mesoscopic imaging method with high specificity and contrast based on optical absorption differences and ultrasound information carriers. This method combines the advantages of high resolution of optical imaging and large penetration depth of ultrasonic imaging. It has been widely studied in the biomedical imaging field. As an important branch of photoacoustic imaging, photoacoustic microscopy can obtain high-resolution and high-contrast images of blood vessels in the dermis layer of the human skin in a noninvasive and label-free manner. Therefore, the use of photoacoustic microscopy was proposed to navigate injection-based microplastic surgeries.

Methods The needle inserted at a fixed angle was imaged using a photoacoustic microscopic probe to obtain the injection point of the needle. Then, the three-dimensional (3D) vascular imaging of the target area was performed. Based on the image fusion and quantitative evaluation, it can be assessed whether the needle will puncture the facial artery, thereby reducing the risk of surgery. In this study, the feasibility of this method is confirmed using leaf vein imaging and *in vivo* mouse-ear imaging. Image reconstructions were performed using a user-defined programme, LABVIEW (2019, National Instruments, USA). The three-dimensional images and image fusion were obtained using functions provided by ImageJ (National Institutes of Health, USA). The user-defined algorithm implemented in MATLAB (R2019b, MathWorks, USA) was used to calculate the number of pixels in the intersection area of the

image fusion.

Results and Discussions Leaf veins were used to simulate the blood vessels of the dermis layer. The diameter of the leaf vein trunk was approximately 300–500 μm (simulating facial arteries) and that of leaf vein branches was <100 μm (simulating capillary networks). The experimental results are consistent with the prediction results of fusion images (Fig. 3). Move the sample matrix to simulate the movement of the sample. The 3D images of the blood vessels in different positions and the needle were fused, and the numbers of pixels in the intersection area were calculated. After image fusion, the numbers of pixels intersecting the vessels (positions 1 and 4) with a diameter of >100 μm are 35 and 31, respectively. The numbers of pixels intersecting the capillaries (positions 2 and 5) are 8 and 5, respectively. The numbers of pixels in positions 3 and 6 without the blood vessels are 0 (Fig. 4).

Conclusions The experimental results of leaf veins show that photoacoustic microscopy can predict the relative position of the needle, simulate the blood vessels, and navigate the needle into a safe area. Results of the *in vivo* mouse-ear experiment show that photoacoustic microscopy can quantitatively determine the type of blood vessel punctured by the needle based on the numbers of pixels in the intersection area. Therefore, this study is expected to realize the preoperative navigation of injection-based microplastic surgeries and shows good application prospects for improving the safety of injection-based microplastic surgeries. However, some aspects still require improvement. The wavelength of the laser employed herein is 532 nm. Naturally, blood shows high absorption at this wavelength; however, the imaging depth is limited owing to the strong scattering of light by biological tissues. Furthermore, high wavelengths of the laser will be used in the future, e.g., 1064 nm, to achieve high imaging depth. Currently, only the upper surface information of the needle can be extracted owing to the limitation by the optical excitation mode of the system; moreover, post-processing algorithms are needed to determine whether the needle touches the blood vessel. In the next step, a complete needle can be simulated using the real size of the needle to improve the accuracy of the experiment. Additionally, there is a certain degree of blindness in the selection of the injection position and the probe must be moved repeatedly. The large imaging view and high imaging speed will considerably improve the detection efficiency. Moreover, owing to the limitation of the imaging speed, the proposed system can only realize preoperative navigation, not intraoperative navigation. Further, this system cannot monitor the process of needle entering the sample in real time. Subsequent work will focus on the aforementioned issues to improve the system.

Key words biotechnology; photoacoustic microscopy; surgical navigation; injection microplastic surgery; image fusion

OCIS codes 170.5120; 510.4030; 520.1040